The X-Discontinuity as a Tracer for Chemical Heterogeneity: Observations from East Africa

Stephen Pugh[1*], Alistair Boyce[1,2], Ian Bastow[3], Cynthia Ebinger[4] and Sanne Cottaar[1]

sdp43@cam.ac.uk, 1. University of Cambridge, 2. Université Claude Bernard, 3. Imperial College London, 4. Tulane University

NERC SCIENCE OF THE ENVIRONMENT

HOMERTON COLLEGE UNIVERSITY OF CAMBRIDGE

1. Introduction

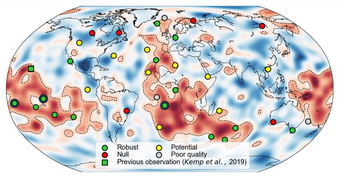

Figure 1. Global distribution of X-discontinuity observations from Pugh et al. (2021) above a depth slice of SEMUCB-WM1 (French & Romanowicz, 2015) at 2800 km depth. Double X observations are marked with two rings.

- Previous observations of the X-discontinuity (~300 km depth) have demonstrated a link between surface hotspot volcanism (Pugh et al., 2021) and thermochemical anomalies in the mantle (Fig. 1).
- Surface volcanism across the African continent (Fig. 2) has been linked to multiple mantle upwellings of varying thermochemical nature.
- Chemical heterogeneities result in seismically observable impedance contrasts meaning receiver functions (RFs) are employed to characterize the nature of the X-discontinuity beneath Africa.

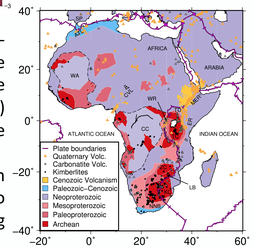

Figure 2. Crustal geology and locations of volcanoes in Africa adapted from Boyce et al. (2021). Black dashed areas mark inferred craton extents now covered by Phanerozoic sediments.

2. Data

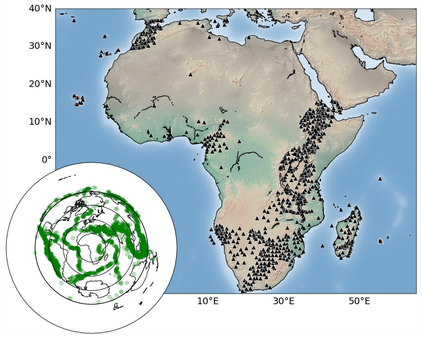

Figure 3. Station (black triangles) and earthquakes (green circles) distribution across the African continent and globe, respectively.

We capitalize on the new TRAILS dataset in the Turkana depression (Bastow, 2019; Ebinger, 2018) to supplement the RF datasets of Boyce & Cottaar (2021) and Pugh et al. (2021). Earthquakes from January 1990 to October 2021 with epicentral distances of 30-90° and $M_W \geq 5.5$ yields >22,500 high quality RFs, recorded at >2,500 stations (Fig. 3).

3. Method

- P to S converted waves (Pds) are generated at seismic discontinuities. RF analysis reveals Pds phases by deconvolving the vertical from the radial seismogram (Fig. 4) using the iterative deconvolution method of Ligorria and Ammon (1999).
- RF are converted to depth using the SEMUCB-WM1 velocity model (French & Romanowicz, 2015).
- High-quality RF are stacked in the time-slowness and depth domains within equidistant bins of radius 111km (~1◦ at the equator) to reveal low amplitude Pds phases, which are discriminated from multiples by their negative slowness (Fig. 5).
- Depth and slowness stacks for each bin are assessed for the presence of the X-discontinuity (272 km; Fig. 6).

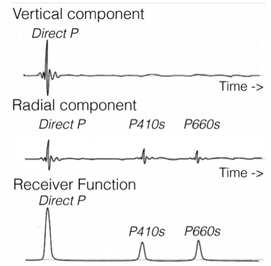

Figure 4. Vertical and radial seismograms and their resultant receiver function. *Courtesy of Jennifer Jenkins.*

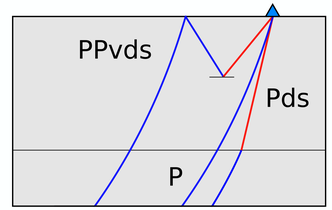

Figure 5. Ray paths of Pds converted phases and shallow bouncing PPvds multiples in the upper mantle. Blue = P-wave, red = S-wave.

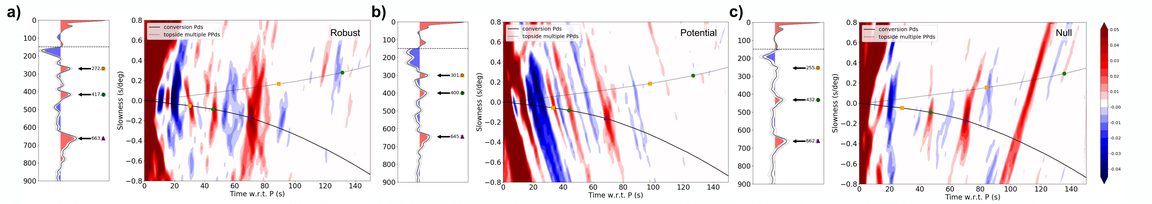

Figure 6. Depth and slowness stacks for 201, 461 and 132 RF with X-discontinuity classifications of a) Robust, b) Potential and c) Null. Symbols mark significant peaks from upper mantle discontinuities (Yellow: X, Green: 410, Purple: 660). Predicted time-slowness curves are shown for the direct (Pds) and multiple (PPvds) phases.

4. Results

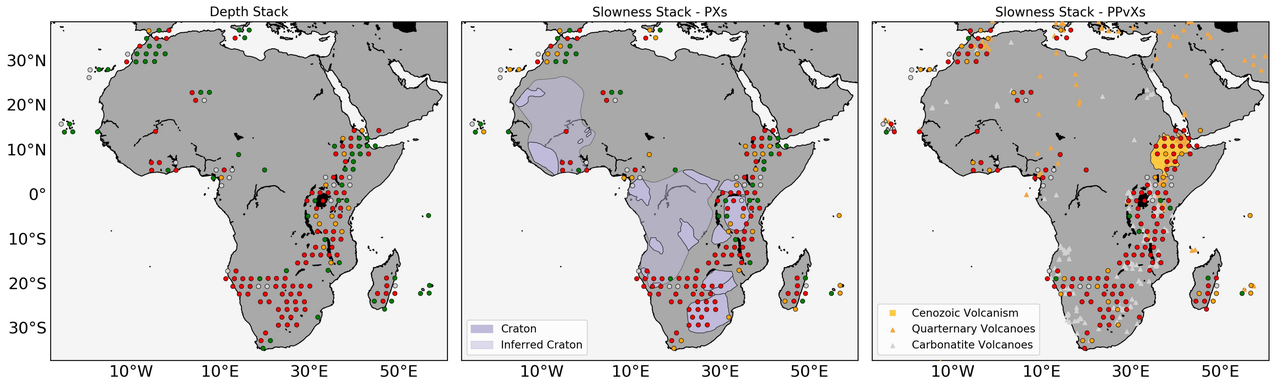

Figure 7. Categorization of the X-discontinuity in 184 bins across Africa (robust = green, potential = orange, null = red and bad quality = grey) for the depth stack, the converted phase in the slowness stack and the multiple from the X-discontinuity in the slowness stack.

- The X-discontinuity is robustly observed in 58 depth stacks, 34 slowness stacks and 9 slowness stacks for the multiple (Fig. 7) at depths of 234 – 319 km.
- The number of RFs within an individual stack has little bearing on the observability of the X-discontinuity, though poor stacks cluster with much fewer RFs than robust, potential, or null stacks (Fig. 8).
- The amplitude and depth of X-discontinuity observations fall within the range of global hotspot observations (Fig. 9; Pugh et al., 2021).
- Observations cluster with sites of active upwelling in the Canary Islands, Cape Verde, Hoggar, Afar, East Africa and Madagascar/Réunion, and subduction beneath Morocco.

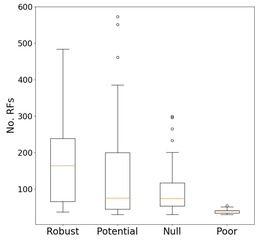

Figure 8. Box plots of the number of RFs for each classification of stack in Fig. 7.

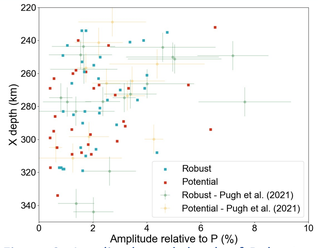

Figure 9. Amplitude and depth of Robust and Potential X-discontinuity observations compared with those of Pugh et al. (2021).

5. Potential Causes

- X-discontinuity depths (234-319 km) have significant overlap with previous studies (285-350 km; Rein et al., 2021, ~250-350km; Owens et al., 2000, 260 & 310 km; Deuss and Woodhouse, 2002) while being observed at shallower depths than before.
- The X-discontinuity has little-to-no correlation with dVs (as a proxy for temperature) suggesting multiple causal mechanisms (Fig. 10).
- In regions of elevated mantle temperatures, the coesite-stishovite phase transition and the formation of carbonated silicate melt are the most plausible causes of the X-discontinuity.
- Whilst overlap occurs between X-discontinuity observations and surface carbonatite melt (Fig. 2), a relationship between the two is yet unconfirmed.
- Other possible causes include the transition of orthoenstatite to high pressure clinoenstatite, though the impedance contrast is expected to be weak.
- Shallow X-discontinuity observations may be associated with a change from anisotropic to isotropic structure linked to the shallower Lehmann discontinuity.

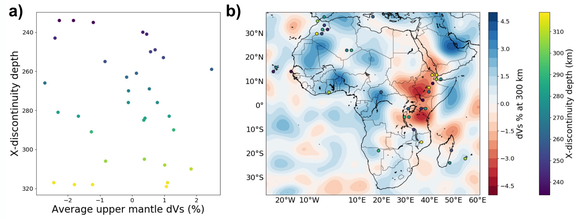

Figure 10. Robust X-discontinuity depths plotted a) against average dVs between 200-400 km from SEMUCB-WM1 and b) spatially above a 300 km depth slice of SEMUCB-WM1.

6. Future Work

- Different tomography models can lead to ≤20 km of discrepancy in depth corrections. RFs corrected with recent highly sampled Africa specific tomographic models (e.g., AFRP20; Boyce et al., 2021) should provide the most robust depth estimates.
- >50% of potential stacks contain strong streaks (Fig. 6b) due to RFs from a narrow epicentral distance range. Incorporation of PP RF into our stacks should help to overcome this.
- Transverse component RFs may reveal the presence of, or lack of, anisotropy in the upper mantle associated with the Lehmann discontinuity.

References

1. Pugh, S., Jenkins, J., Boyce, A. and Cottaar, S., 2021. Global receiver function observations of the X-discontinuity reveal recycled basalt beneath hotspots. Earth Planet. Sci. Lett.
2. French, S.W. and Romanowicz, B. A., 2014. Whole-mantle radially anisotropic shear velocity structure from spectral-element waveform tomography. Geophys. J. Int.
3. Kemp, M., Jenkins, J., Maclennan, J. and Cottaar, S., 2019. X-discontinuity and transition zone structure beneath Hawaii suggests a heterogeneous plume. Earth Planet. Sci. Lett.
4. Boyce, A., Bastow, I.D., Cottaar, S., Kounoudis, R., Guilloud De Courbeville, J., Caunt, E. and Desai, S., 2021. AFRP20: New P-Wavespeed Model for the African Mantle Reveals Two Whole-Mantle Plumes Below East Africa and Neoproterozoic Modification of the Tanzania Craton. Geochem. Geophys. Geosyst.
5. Bastow, Ian and Ayele, Atalay (2019) Northern Lake Abaya Broadband Network [Data set].
6. Cynthia Ebinger. (2018). Crust and mantle structure and the expression of extension in the Turkana Depression of Kenya and Ethiopia [Data set].
7. Boyce, A. and Cottaar, S., 2021. Insights Into Deep Mantle Thermochemical Contributions to African Magmatism From Converted Seismic Phases. Geochem. Geophys. Geosyst.
8. Ligorría, J.P. and Ammon, C.J., 1999. Iterative deconvolution and receiver-function estimation. Bull. Seismol. Soc. Am.
9. Rein, T., Hannemann, K., Thomas, C. and Korn, M., 2020. Location and characteristics of the X-discontinuity beneath SW Morocco and the adjacent shelf area using P-wave receiver functions. Geophys. J. Int.
10. Owens, T.J., Nyblade, A.A., Gurrola, H. and Langston, C.A., 2000. Mantle transition zone structure beneath Tanzania, East Africa. Geophys. Res. Lett
11. Deuss, A. and Woodhouse, J.H., 2002. A systematic search for mantle discontinuities using SS-precursors. Geophys. Res. Lett

Funding Statement

S. Pugh acknowledges support from **Natural Environment Research Council** grant number NE/L002507/1. A. Boyce and S. Cottaar are funded by **Natural Environment Research Council** grant NE/R010862/1, S. Cottaar is funded by the **European Research Council** under the EU's Horizon 2020 programme (grant 804071-ZoomDeep) and A. Boyce is supported by the **Centre National de la Recherche Scientifique** at unit UMR5276 (LGL-TPE). I. D. Bastow acknowledges support from **Natural Environment Research Council** grant number NE/S014136/1. C. Ebinger acknowledges **National Science Foundation** NSFGEO-NERC award 1824417. The facilities of **IRIS Data Services**, and specifically the **IRIS Data Management Center**, were used for access to waveforms, related metadata, and/or derived products used in this study. IRIS Data Services are funded through the Seismological Facilities for the Advancement of Geoscience (SAGE) Award of the **National Science Foundation** under Cooperative Support Agreement EAR-1851048.